

1-21-2021

## The Status of Air Quality in the United States During the COVID-19 Pandemic: A Remote Sensing Perspective

Yasin F. Eishorbany  
*University of South Florida*

Hannah C. Kapper  
*University of South Florida*

Jerald R. Ziemke  
*NASA Goddard Space Flight Center*

Scott A. Parr  
*Embry-Riddle Aeronautical University*

Follow this and additional works at: [https://digitalcommons.usf.edu/usf\\_fcrc\\_all](https://digitalcommons.usf.edu/usf_fcrc_all)

---

### Scholar Commons Citation

Eishorbany, Yasin F.; Kapper, Hannah C.; Ziemke, Jerald R.; and Parr, Scott A., "The Status of Air Quality in the United States During the COVID-19 Pandemic: A Remote Sensing Perspective" (2021). *All publications*. 1.  
[https://digitalcommons.usf.edu/usf\\_fcrc\\_all/1](https://digitalcommons.usf.edu/usf_fcrc_all/1)

This Article is brought to you for free and open access by the USF Libraries Florida COVID-19 Research Collections at Digital Commons @ University of South Florida. It has been accepted for inclusion in All publications by an authorized administrator of Digital Commons @ University of South Florida. For more information, please contact [digitalcommons@usf.edu](mailto:digitalcommons@usf.edu).



## Article

# The Status of Air Quality in the United States During the COVID-19 Pandemic: A Remote Sensing Perspective

Yasin F. Elshorbany <sup>1,\*</sup>, Hannah C. Kapper <sup>1</sup>, Jerald R. Ziemke <sup>2,3</sup> and Scott A. Parr <sup>4</sup>

<sup>1</sup> College of Arts and Sciences, University of South Florida, St. Petersburg, FL 33701, USA; hannahkapper@usf.edu

<sup>2</sup> NASA Goddard Space Flight Center, Greenbelt, MD 20771, USA; jerald.r.ziemke@nasa.gov

<sup>3</sup> Goddard Earth Sciences Technology and Research (GESTAR), Columbia, MD 21046, USA

<sup>4</sup> Department of Civil Engineering, Embry-Riddle Aeronautical University, Daytona Beach, FL 32114, USA; PARRS1@erau.edu

\* Correspondence: elshorbany@usf.edu

**Abstract:** The recent COVID-19 pandemic has prompted global governments to take several measures to limit and contain the spread of the novel virus. In the United States (US), most states have imposed a partial to complete lockdown that has led to decreased traffic volumes and reduced vehicle emissions. In this study, we investigate the impacts of the pandemic-related lockdown on air quality in the US using remote sensing products for nitrogen dioxide tropospheric column (NO<sub>2</sub>), carbon monoxide atmospheric column (CO), tropospheric ozone column (O<sub>3</sub>), and aerosol optical depth (AOD). We focus on states with distinctive anomalies and high traffic volume, New York (NY), Illinois (IL), Florida (FL), Texas (TX), and California (CA). We evaluate the effectiveness of reduced traffic volume to improve air quality by comparing the significant reductions during the pandemic to the interannual variability (IAV) of a respective reference period for each pollutant. We also investigate and address the potential factors that might have contributed to changes in air quality during the pandemic. As a result of the lockdown and the significant reduction in traffic volume, there have been reductions in CO and NO<sub>2</sub>. These reductions were, in many instances, compensated by local emissions and, or affected by meteorological conditions. Ozone was reduced by varying magnitude in all cases related to the decrease or increase of NO<sub>2</sub> concentrations, depending on ozone photochemical sensitivity. Regarding the policy impacts of this large-scale experiment, our results indicate that reduction of traffic volume during the pandemic was effective in improving air quality in regions where traffic is the main pollution source, such as in New York City and FL, while was not effective in reducing pollution events where other pollution sources dominate, such as in IL, TX and CA. Therefore, policies to reduce other emissions sources (e.g., industrial emissions) should also be considered, especially in places where the reduction in traffic volume was not effective in improving air quality (AQ).

**Keywords:** COVID-19 pandemic; US; air quality; remote sensing; atmospheric composition



**Citation:** Elshorbany, Y.F.; Kapper, H.C.; Ziemke, J.R.; Parr, S.A.

The Status of Air Quality in the United States During the COVID-19 Pandemic: A Remote Sensing Perspective. *Remote Sens.* **2021**, *13*, 369. <https://doi.org/10.3390/rs13030369>

Received: 4 December 2020

Accepted: 18 January 2021

Published: 21 January 2021

**Publisher's Note:** MDPI stays neutral with regard to jurisdictional claims in published maps and institutional affiliations.



**Copyright:** © 2021 by the authors. Licensee MDPI, Basel, Switzerland. This article is an open access article distributed under the terms and conditions of the Creative Commons Attribution (CC BY) license (<https://creativecommons.org/licenses/by/4.0/>).

## 1. Introduction

The COVID-19 pandemic has led to profound impacts on the global population, resulting in almost a million deaths in addition to several millions of infected people, many of whom are still suffering from various side effects despite surviving the novel virus [1]. Governments around the globe have enforced several measures to contain the spread of the virus. In the United States (US), ~8 million people were infected, and there were ~200 k total deaths as of October 2020 [2]. The White House declared a state of emergency on 13 March 2020, and travel restrictions were applied. On 16 March 2020, the White House advised against large gatherings, and since 19 March 2020, the State Department has advised US citizens to avoid all international travel [3].

The impact of COVID-19 on general mobility has been staggering. A survey conducted in the Netherlands found that 80% of respondents actively reduced their outdoor, and the number of trips taken reduced by 55% [4]. Further survey results from Australia found household trips reduced by over 50% across all modes, and the proportion of transit trips decreased from a pre-lockdown level of 14% to just 7% [5]. A study of roadway detectors in Florida (FL) found that vehicle volumes across the state had dropped by 47.5% [6]. Recent studies have also attempted to correlate mobility habits and the proliferation of COVID-19. In Italy, the number of daily new COVID-19 cases was related to trips performed three weeks earlier [7], and another study in the United Kingdom found that mobility reductions had a significant impact on reducing COVID-19 [8].

The COVID-19 related lockdown measures have resulted in a decrease in traffic volume and other economic activities and their related anthropogenic emissions. Traffic emissions are a primary source of carbon monoxide (CO), nitrogen oxide (NO), and nitrogen dioxide (NO<sub>2</sub>) [9–11]. While CO and NO are emitted directly from vehicle emissions, NO<sub>2</sub>, ozone (O<sub>3</sub>), and secondary organic and inorganic aerosols are mainly photochemical products, and their atmospheric concentration and lifetime depend on the non-linear chemistry of O<sub>3</sub>, NO<sub>x</sub> (NO<sub>x</sub> = NO + NO<sub>2</sub>), and volatile organic compounds (VOCs) in addition to the oxidant's levels, meteorology, and solar radiation [12]. Several recent studies have reported improved air quality (AQ) due to the pandemic related lockdown [13–16]. In most studies, the change in air pollutants due to the lockdown was calculated by comparing the pollutant concentration during the lockdown to that of a previous base period of time or model simulations [14,15]. However, there are large discrepancies within the literature regarding the representativeness and the time duration of lockdown and base periods. For instance, some studies use a lockdown period of January to May [14], while others use much shorter periods [16]. The time duration of the base periods also varied within the literature from few months [17] to several years [18,19], which makes the comparison between different studies regarding the relative impacts of COVID-19 burdensome. For example, [18] concluded, based on data from ground-based monitoring network stations, that reductions in air pollution during a five months lockdown period in New York City (NYC) are within the interannual variability of the last five years (2015–2019). Other studies used only a few months to one year as a reference period [20–23].

Ref. [24] investigated the ozone photochemical formation in Quito, Ecuador, using a photochemical box model based on the reduction of the NO during the rush hour time during the pandemic compared to the levels before the pandemic. The reduction in NO revealed a significant increase in ozone production. [25] reported several periods of heavy haze pollution in east China during the lockdown and concluded that enhanced secondary pollution might have offset reduction of primary emissions in China. [25] found that reduction of NO<sub>x</sub> emissions during the pandemic increased ozone and nighttime NO<sub>3</sub> radicals and thus increase the nighttime atmospheric oxidation capacity, facilitating the formation of secondary organic and inorganic particulate matter [25]. The results of [25,26] indicate that the severe pollution episode was still happening during the pandemic despite decreased emissions from traffic and other economic sectors. These results show the importance of accounting for the formation of secondary oxidation products as well as other emissions sources when discussing the impacts of reduction in traffic emissions.

In FL, using ground-based measurements, [27] found a reduction in NO<sub>2</sub>, CO, and O<sub>3</sub> but an increase in SO<sub>2</sub> and PM<sub>2.5</sub> during the first two weeks of April, which they related to increased power consumption during the lockdown period. In NYC, while [18] found no significant differences, [14,28] found a significant reduction in NO<sub>2</sub> and O<sub>3</sub> in both NYC and FL.

In this study, we use actual traffic data to estimate the lockdown period, and we use remote sensing products that have coverage of several years before the 2020 COVID-19 pandemic to evaluate the AQ changes as well as the effectiveness of the reduction in traffic volume on AQ in several states with diverse geographic and environmental conditions. We investigate the impacts of the pandemic-related lockdown on AQ in the US

and consequently focus on regions with a distinctive anomaly, New York (NY), Illinois (IL), FL, Texas (TX), and California (CA).

## 2. Methodology

### 2.1. Traffic Volume and COVID-19 Cases

The Federal Highway Administration (FHWA) directs state departments of transportation to provide annual traffic statistics [29]. State transportation agencies are responsible for building, operating, and maintaining permanent traffic monitoring stations to collect a variety of traffic statistics, including traffic count information. Continuous count stations collect hourly traffic counts throughout the year to meet the federal requirements of the National Highway Performance Monitoring System (HPMS). The states analyzed in this study have made their traffic information available through their websites (NY), through data requests (FL), or third-party vendors (IL and Massachusetts (MA)). Bidirectional hourly traffic counts were collected, cataloged, and processed from hundreds of telemetric monitoring stations. The data were reviewed for errors. A common error was missing data and/or sites reporting zero values. The zero values were attributable to road closures because of incidents, scheduled maintenance work, and malfunctioning roadway sensors. Sites with three or more consecutive observations of zero values were removed. We also used available literature to investigate the traffic volume for California [30].

### 2.2. Remote Sensing Products

In this section, we describe the different satellite products used in this study. A list of these products is shown in Table 1.

**Table 1.** Data products and their reference periods.

Parameter	Resolution	Instrument/Platform	Reference Period
NO <sub>2</sub>	0.1°	OMI/Aura	2015–2019
CO	1°	MOPITT/TERRA	2015–2019
AOD	1°	MODIS DB land/TERRA	2010–2019
Ozone	1°	OMPS/MERRA-2	2015–2019

AOD: aerosol optical depth; DB: deep blue; OMPS: ozone mapping profiler suite; MERRA-2: modern-era retrospective analysis for research and applications-2.

#### 2.2.1. Nitrogen Dioxide (NO<sub>2</sub>)

NO<sub>2</sub> tropospheric column data was obtained from the OMI instrument aboard the Aura satellite. Aura was launched into a sun-synchronous, near-polar orbit in July 2004. It orbits at 705 km (438 miles) above the Earth with a sixteen-day repeat cycle, and it has a 1:45 PM ± 15 min equator crossing time. With its 2600 km wide swath on the surface, OMI measurements have a daily global coverage. Daily OMI NO<sub>2</sub> L3 V4 gridded data was obtained at 0.1° resolution from NASA Goddard Earth Sciences Data and Information Services Center [31].

#### 2.2.2. Carbon Monoxide (CO)

CO atmospheric column gridded daily means were obtained from the MOPITT instrument aboard the Terra Satellite [32,33]. Terra was launched into a sun-synchronous polar orbit in December 1999. Terra orbits at 705 km with a sixteen-day repeat cycle and crosses the equator at approximately 10:30 am. Daily L3 V008 data was obtained at 1° resolution from the NASA Langley Research Center Atmospheric Science Data Center (ASDC).

#### 2.2.3. Aerosol Optical Depth (AOD)

Aerosol optical depth, AOD, is a measure of the aerosol load in the atmosphere, and it represents the degree to which aerosols prevent the transmission of light in the atmosphere. AOD of less than 0.1 indicates a clear sky with maximum visibility, whereas

a value of 4 indicates a high dense aerosol load that obstructs vision. In this study, we used the MODIS (Terra) Collection 6.1 aerosol products datasets, which were obtained at Level 3 from the Atmosphere Archive and Distribution System (LAADS) Distributed Active Archive Center (DAAC) and has been recently validated [34–36]. We used product MOD08\_D3, which is a daily 1° product. MODIS, with its 2330 km viewing swath width, provides almost daily global coverage. We used the MODIS Deep Blue (DB) aerosol product (Deep\_Blue\_Aerosol\_Optical\_Depth\_550\_Land\_Mean). The DB algorithm is preferable for bright-reflecting land surfaces, such as semiarid and urban/industrial regions [35].

#### 2.2.4. Tropospheric Ozone Column (O<sub>3</sub>)

We used the tropospheric column ozone (TCO) product derived by combining total column ozone from the Suomi National Polar-orbiting Partnership (NPP) Ozone Mapping Profiler Suite (OMPS) nadir-mapper (NM) v2.1 total ozone [37,38] with stratospheric column ozone from Modern-Era Retrospective analysis for Research and Applications-2 (MERRA-2) [39], both of which have been evaluated and validated, and are in the public domain [40]. We also included extensive comparisons between OMPS/MERRA-2 TCO and ozonesonde (Figures S1 and S2) and OMI/MLS TCO (Figures S3 and S4). Footprint measurements of tropospheric ozone were binned to 1° latitude × 1° longitude resolution. MERRA-2 assimilated stratosphere column ozone was found to agree within ±2–3 Dobson Units (DU) with original MLS along-track measurements from tropics to high latitudes. Comparisons between collocated ozonesonde and OMPS/MERRA-2 TCO in the tropics and extra-tropics indicate that mean differences varied from near zero to at most ~±6 DU, respectively, with standard deviations from a few DU in the tropics to at most ~6–8 DU in mid-high latitudes (Figures S1 and S2). Similarly, mean offsets between OMI/MLS and OMPS/MERRA-2 TCO were small, at most 2–3 DU everywhere except in mid-high latitudes in the southern hemisphere (SH) where the average offset was about −5 DU, with small difference standard deviations of only about 2–3 DU at all latitudes. These small standard deviations show that the two TCO products were capturing very similar space-time variability (Figure S4).

### 2.3. Analysis Period and Data Significance

#### 2.3.1. Analysis Period

To estimate the anomaly in the pollutant's levels, we compare the pollutant concentration in 2020 to a base period represented by a reasonable number of previous years. For NO<sub>2</sub>, CO, and O<sub>3</sub>, we used a base period of five years (2015–2019). For AOD, we use a base period of ten years (2010–2019) as a representative mean [41]. Furthermore, the MODIS AOD DB algorithm [35], used in this study, has been reported to underestimate PM<sub>2.5</sub> in the AOD range of 0–0.5 by ~22% [42]. Therefore, a reduction of AOD by up to ~20% less than the interannual variability (IAV) was considered carefully in this study and will not be considered a significant reduction.

#### 2.3.2. Data Significance

We evaluated the significance of the results using two approaches:

**Statistical Significance:** We calculated the statistical significance of the difference between the daily base and lockdown periods at each grid point using the two *t*-test hypotheses [43] at a confidence limit of 95%. Significant relative changes (*sig* Δ), calculated as (2020 – base)/base × 100, shown in the following sections, include only significant differences.

**Detrended Interannual Variability (IAV):** This large-scale experiment presented an unprecedented opportunity to investigate the potential of reducing traffic emissions on AQ. To evaluate the potential of these emission reductions on AQ in comparison to the previous years, we compared the *sig* Δ related to the pandemic to the detrended IAV of the base period. We calculated the effectiveness of the reduction in traffic volume (ETR) to reduce air pollutants during the pandemic,  $ETR = -sig \Delta - IAV$ . This relation applies only to a

reduction in air pollutants (*sig*  $\Delta$  should be negative) since an increase in pollutant levels is not related to the lockdown but to other factors, such as pollution events, as discussed below. An ETR value of  $\leq 0$  indicates that traffic reduction during the lockdown was not effective in improving the AQ. A positive ETR implies that the reduction in traffic emissions in these regions is effective in improving AQ. Although these significant reductions in traffic volume of up to 60% (see Section 3.1) may not be achievable in normal circumstances, it provides decisions makers with valuable information to guide policies regarding traffic emissions.

We calculated the IAV by removing the long-term historical trends from the non-stationary time series. The variability for non-stationary data includes variability due to historical trends in addition to the IAV. To differentiate the IAV from historical trends, we (1) applied polynomial regression analyses to calculate the trend of the time series, (2) calculated the IAV as the difference of the fitted data from the original data, and (3) calculated the standard deviation of the difference, which is a measure of the IAV. Other methods for calculating the trend, such as calculating the running mean of non-stationary time series or the empirical mode decomposition method, were mainly used for decadal-scale climatic trends [44–46].

### 3. Results and Discussion

In the following sections, we, (1) discussed the reduction in traffic volume as a result of the pandemic related lockdown (Section 3.1), (2) investigated the large-scale impacts of lockdown on AQ in the US (Section 3.2), and (3) consequently focused on the following regions and states (between brackets) where the changes were significant (Section 3.3): northeast (NY), Midwest (IL), southeast (FL), south (TX), west coast (CA) (Figure 1).



**Figure 1.** Locations of the US cities investigated in this study.

#### 3.1. Traffic Volume and COVID-19 Cases in the US

Since the most reported pandemic-related effect on AQ was the reduction in traffic volume during lockdown periods, we investigated the changes in traffic volume during the pandemic and its relation to air quality. We calculated the relative change in the number of vehicles related to the same period in 2019 rather than prior to the lockdown period since it accounts for the seasonal variability of the vehicle traffic as well. The analysis investigated differences in traffic occurring on similar days, i.e., matched days of the week. For example, traffic from the first Monday in March of 2020 was compared to traffic on the first Monday in March of 2019. Therefore, the comparison period was 1 March 2020–31 May 2020 and 3 March 2019–2 June 2019 to account for this offset. Within each state, traffic counts at unique locations from 2020 were compared to 2019 levels using a paired *t*-test. Statistically significant changes in traffic (at 95% confidence limit) in 2020 were first observed on 11 March in FL, 12 March in MA, and 13 March in NY, and IL.

Figure 2 shows that the minimum number of vehicles occurs after several weeks of imposing the lockdown in most states, which is an important aspect that should be considered in the calculation of the analysis period for AQ analyses. The relative maximum reduction in the number of vehicles in most states was about 60% (Figure 2), except in IL (only ~40%). The maximum reduction in the traffic volume did not coincide all the time with the maximum number of cases. For example, in MA and IL, the number of cases continued to increase despite the lockdown and the near-stagnant traffic. In contrast, in FL

and NY, the maximum reduction of traffic volume coincides with the maximum number of cases. Based on the decrease in the traffic volume, we determine a common effective lockdown period from 1 April to 1 May for all investigated states (Figure 2). Henceforth, the effective lockdown period is referred to by the term “lockdown period”. The number of grounded vehicles due to the lockdown measures did not return to its levels before the pandemic despite increasing gradually from 1 May.

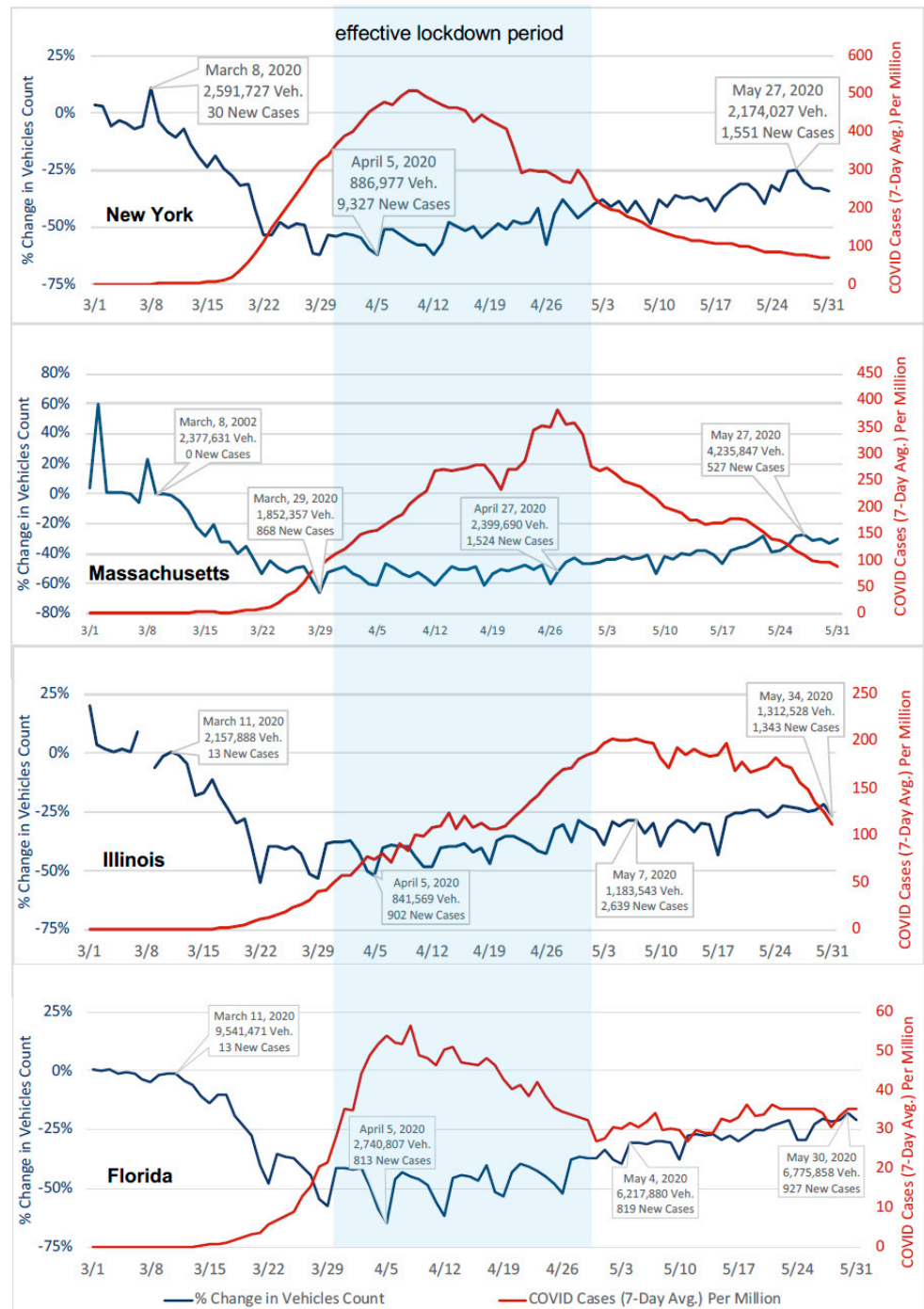


Figure 2. Seven day rolling average of new COVID-19 cases per million in population and change in Table, 2020 vs. 2019).

### 3.2. An Overview of Air Quality Tracers in the US

The COVID-19 related lockdown led to a reduction in traffic volume by 40–60% in most states (Section 3.1). Anthropogenic emissions are highest in the northeast (NE) and Midwest of the US, in addition to CA and TX [47]. Emissions from the transportation sector, which includes motor vehicle fuel, motor vehicle manufacturing, air travel direct and indirect emissions, and public transit, account for ~28% of the total emissions, with light- and heavy-duty vehicles accounting for most of these emissions [47,48]. In this study, we evaluate the changes in pollutant concentrations. We note that pollutant concentrations depend on other factors, in addition to transportation emissions such as emissions from other sources, short- and long-range transport, and loss processes and chemical transformations that are in turn affected by meteorological parameters such as temperature, humidity, and solar radiation.

#### 3.2.1. Spatial Distribution

Figure 3 shows the base  $\text{NO}_2$ , CO,  $\text{O}_3$ , AOD levels, the IAV of the base period, and the  $\text{sig } \Delta$  due to the lockdown period during the COVID-19 pandemic. Pollutant concentrations are lower on high elevation sites, the Sierra Nevada, and the Rocky Mountains in the west, and the Appalachian Mountains in the east (Figure 3).  $\text{NO}_2$  is mainly an atmospheric photochemical oxidation product of NO reaction with VOCs ( $\text{RO}_2/\text{HO}_2 + \text{NO} \rightarrow \text{NO}_2$ ). Traffic is the primary source of NO.  $\text{NO}_2$  levels have been reported to be significantly decreased in different places around the world during the COVID-19 pandemic [14–18].  $\text{NO}_2$  levels in the US are largest in the NE, including NY and Massachusetts (MA), due to the high NO and VOC emissions in this region [47,49]. CO, a primary anthropogenic pollutant, reached its maximum in the NE with relatively high concentrations in the Midwest and west coast of the US (Figure 3).  $\text{O}_3$  is a photochemical secondary oxidation product that results from  $\text{NO}_2$  photolysis. Therefore,  $\text{O}_3$  was higher in the southern part of the US where higher solar radiation and temperature favor ozone formation. Ozone formation depends on  $\text{NO}_x$  and VOC levels as well as the sensitivity to the photochemical regime [50]. The reduction of  $\text{NO}_2$  levels under NO sensitive conditions may lead to decreased  $\text{O}_3$  levels, while under VOC-sensitive conditions, ozone increases as  $\text{NO}_2$  decreases [50]. The pollution levels in the US have declined significantly over the last few decades [51,52], which led to several regions becoming NO-sensitive, except during special pollution events. Furthermore, during the summer months in the northern hemisphere, the boundary layer height (BLH) is deeper, and NO mixing ratios are lower compared to winter. AOD was also high along the eastern and the southern coasts, including FL and south TX.

#### 3.2.2. Interannual Variability and Significant Changes during the Lockdown

We used the IAV to evaluate the reduction of pollutants levels during the lockdown compared to the previous years, i.e., how effectively the reduction in traffic volume improved AQ (see Section 2.3.2). The detrended IAV (see Section 2.3) was lower than the total variability (see Supplementary), which included variability due to historical trends and IAV. The  $\text{NO}_2$  IAV was highest in the northern US and lowest in the south, related to the higher photolysis rate and shorter lifetime in the south compared to the north (Figure 3). The relative change of the  $\text{NO}_2$  due to the pandemic seemed to be within the interannual variability (up to  $\pm 20\%$ ) in most of the US but higher (up to  $-50\%$ ) in few other places (e.g., NYC, FL, and CA). As shown in Figure 3, the IAV of CO over most of the US was  $<10\%$ , which was relatively small, and with no clear latitudinal trend as in  $\text{NO}_2$ . This due to  $\text{NO}_2$  being a photochemical product while CO is primarily emitted, mainly from fuel combustion, with a much longer atmospheric lifetime compared to  $\text{NO}_2$  [53]. As demonstrated in Figure 3, CO relative changes over most of the US were within the IAV, except for a few places, which we investigated further in the next sections.

Similar to CO, ozone IAV was lower than that of  $\text{NO}_2$  and was slightly higher in the east, especially over FL ( $\sim 7\%$ ) compared to the west ( $\sim 3\%$ ). The low variability of ozone was due to the presence of significant ozone background levels over the US [54].

The relative reduction (*sig Δ*) in O<sub>3</sub> due to the pandemic is most significant in the eastern US, including FL (Figure 3).

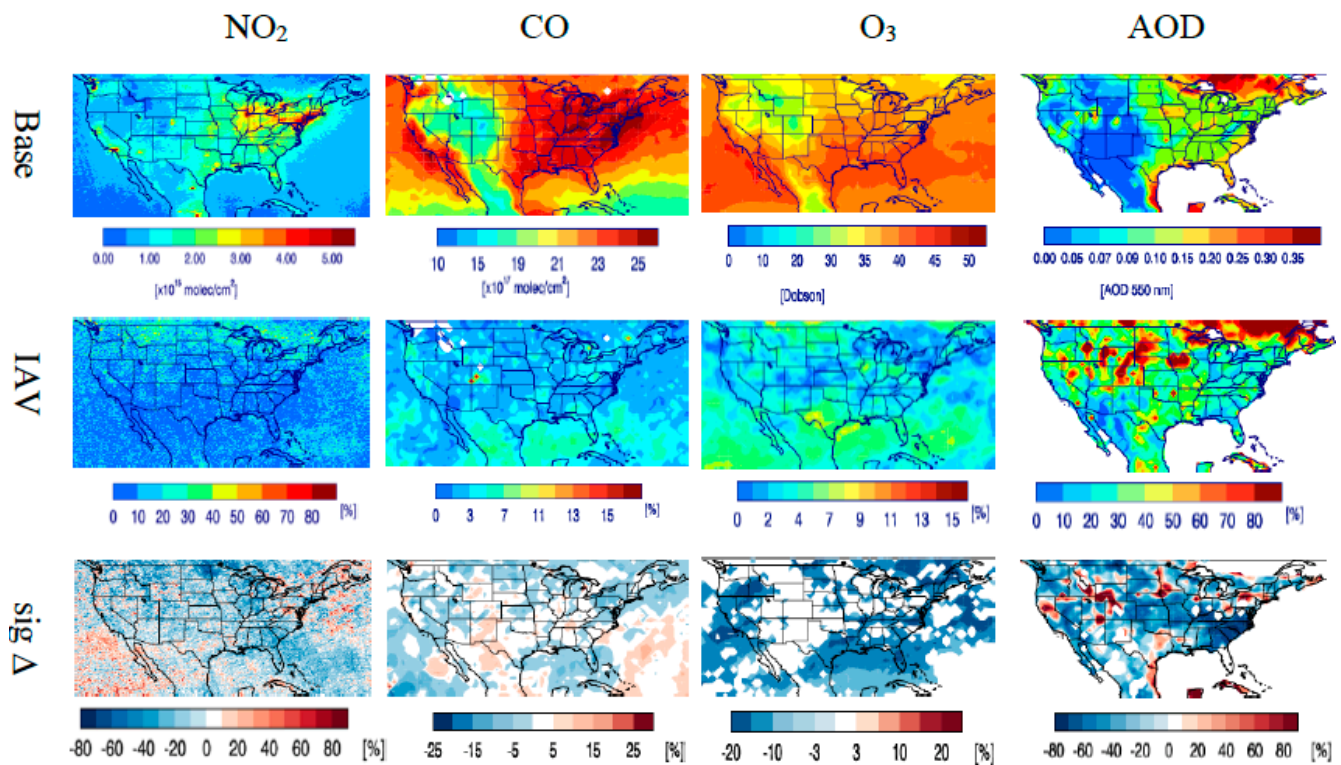


**Figure 3.** Top panel: Mean pollutant levels during the base period (Base); Middle panel: detrended Interannual Variability (IAV) of the base period; Bottom panel: Significant relative change (*sig Δ*) during the lockdown period of the COVID-19 pandemic. Blank areas in the last row (*sig Δ*) refers to insignificant differences.

IAV of AOD seemed to vary much larger compared to CO and NO<sub>2</sub>, ranging from 10% in northern FL to 80% in the north and northwest of the US (Figure 3). This was due to the different aerosol sources from primary emissions, long-range transport (especially on the western coast [55]), atmospheric oxidation, the aerosol dependency on meteorology such as relative humidity, and BLH [56,57]. AOD measures the levels of organic and inorganic aerosols. Secondary organic aerosol (SOA) formation increases in aged air masses as a result of the photochemical oxidation of primary organic aerosols (OA) [55]. While inorganic sulfate aerosol formation can be oxidant (O<sub>3</sub> or H<sub>2</sub>O<sub>2</sub>)- or SO<sub>2</sub> limited, the formation of nitrate aerosols depends on the uptake of HNO<sub>2</sub> into the cloud or aerosol particles and its reaction with ammonium or other cations [53]. In ammonia-limited regions (such as coastal areas), enhanced sulfates substitute for nitrate and chloride ions in the aerosol particles. Therefore, the formation of new aerosol particles and, or the change in the chemical composition of the existing aerosols depends on the interplay of these factors in each region. Recent studies showed discrepancies between MODIS AOD values and ground-based measurement of the aerosol mass concentrations in China during the pandemic, which the authors relate to the variable meteorological conditions, such as water content, which lead to an inaccurate evaluation of surface aerosols [56]. Ref. [56] found a weaker PM<sub>2.5</sub>/AOD ratio in coastal areas and higher in winter and lower in summer. Ref. [42] reported that, compared to AERONET AOD, MODIS AOD datasets generated by the deep blue algorithm (used in this study) are negatively biased by ~22% in the AOD range of 0–0.5 while the dark target algorithm and the merged dataset are positively biased. AOD *sig Δ* was highest on the eastern and western coasts, while no *sig Δ* can be detected in FL (Figure 3).

Generally, the lockdown period has a variable impact on the NO<sub>2</sub>, O<sub>3</sub>, CO, and AOD, which we investigated their spatial patterns in each region in the following sections. We also show daily time series plots for IAV of tropospheric NO<sub>2</sub> and O<sub>3</sub> column (there are no sufficient data to construct time series for CO and AOD) in select cities. O<sub>3</sub> data of 1° resolution were not sufficient to calculate the 0.5° box, which would have been more representative for urban traffic changes around city centers. Therefore, plots were calculated using the mean of a 1° box around selected cities for both O<sub>3</sub> and NO<sub>2</sub> (for consistency with O<sub>3</sub>). Therefore, these plots reflect more of a regional rather than an urban pattern.

### 3.3. Regional Impacts

Based on the overview analysis of pollutants level and variability over the US (Section 3.2), we determined five regions where changes during the COVID-19 lockdown were significant. In the following sections, we investigated the changes in each region and highlighted the main reason for these significant changes.

#### 3.3.1. Northeast

Anthropogenic concentrations of CO and NO<sub>x</sub>, and VOC are highest in this part of the US. In NYC, the NO<sub>2</sub> IAV is up to ~20%, and NO<sub>2</sub> reduction (*sig Δ*) is ~50% (see Figure 4), which is in agreement with ground-based measurements [14,58]. ETR(NO<sub>2</sub>) was ~30% (i.e., 30% reduction beyond the IAV). Therefore, we could conclude that the reduction in traffic volume in NYC during the lockdown was effective in reducing NO<sub>2</sub> by ~30% compared to the base period. As shown in Figure 5, the reduction of NO<sub>2</sub> in NYC during the pandemic, compared to the mean IAV of the base period, was the highest among all investigated cities (Figure 5), in agreement with ground-based measurement [14]. Ref. [58] also used ground-based measurements and a lockdown period from 13 March to 21 April, and found a statistically significant reduction in NO<sub>2</sub>, in agreement with our results. The reduction in NO<sub>2</sub>, as demonstrated in the spatial analysis (Figure 4), also agrees with [14], who found significant NO<sub>2</sub> reduction over NYC using both satellite and ground-based measurements. Downwind of NYC, NO<sub>2</sub> IAV reached up to 30%, with a relative change of up to 60%. Also, in Charleston, West Virginia (WV), there was an increase of NO<sub>2</sub> of up to ~20%, which was likely due to local industrial emissions from nearby heavy industrial parks [59,60] but well within the IAV (ETR is ≤0). As shown in Figure 5, NO<sub>2</sub> was slightly increased (compared to the mean IAV of the base period) in Charleston, WV, during the first two weeks and then decreased in the second two weeks of April. The increase in NO<sub>2</sub> was not related to the reduction in traffic volume. In Ithaca, NY, there was a decrease in NO<sub>2</sub> IAV during the pandemic. In New Jersey (NJ), and Delaware (DE), the IAV was much less at ~15%, and the NO<sub>2</sub> reduction due to the pandemic was also ~15%, ETR is ≤0. Therefore, we conclude that reduction in traffic volume in these states was not as effective in improving AQ as in NYC, which was due to the much lower traffic volume in these states compared to NY [29]. Overall, the reduction of traffic volume during the COVID-19 pandemic in the NE US was effective in reducing NO<sub>2</sub> compared to IAV only in NYC.

CO has a longer atmospheric lifetime than NO<sub>2</sub>, so the impact of emission changes would be less localized than for NO<sub>2</sub>. CO IAV was low at ~2% over NY and NJ and DE. A CO *sig Δ* of −15% over NY during the lockdown was evident, and was higher than the 3% IAV, ETR = 12% (see Figure 4). Over New Jersey and Delaware, relative *sig Δ* of −5% was well within the IAV values, and so ETR is ≤0. Therefore, the reduction in traffic volume in NYC is also effective in reducing CO levels, compared to the base period.

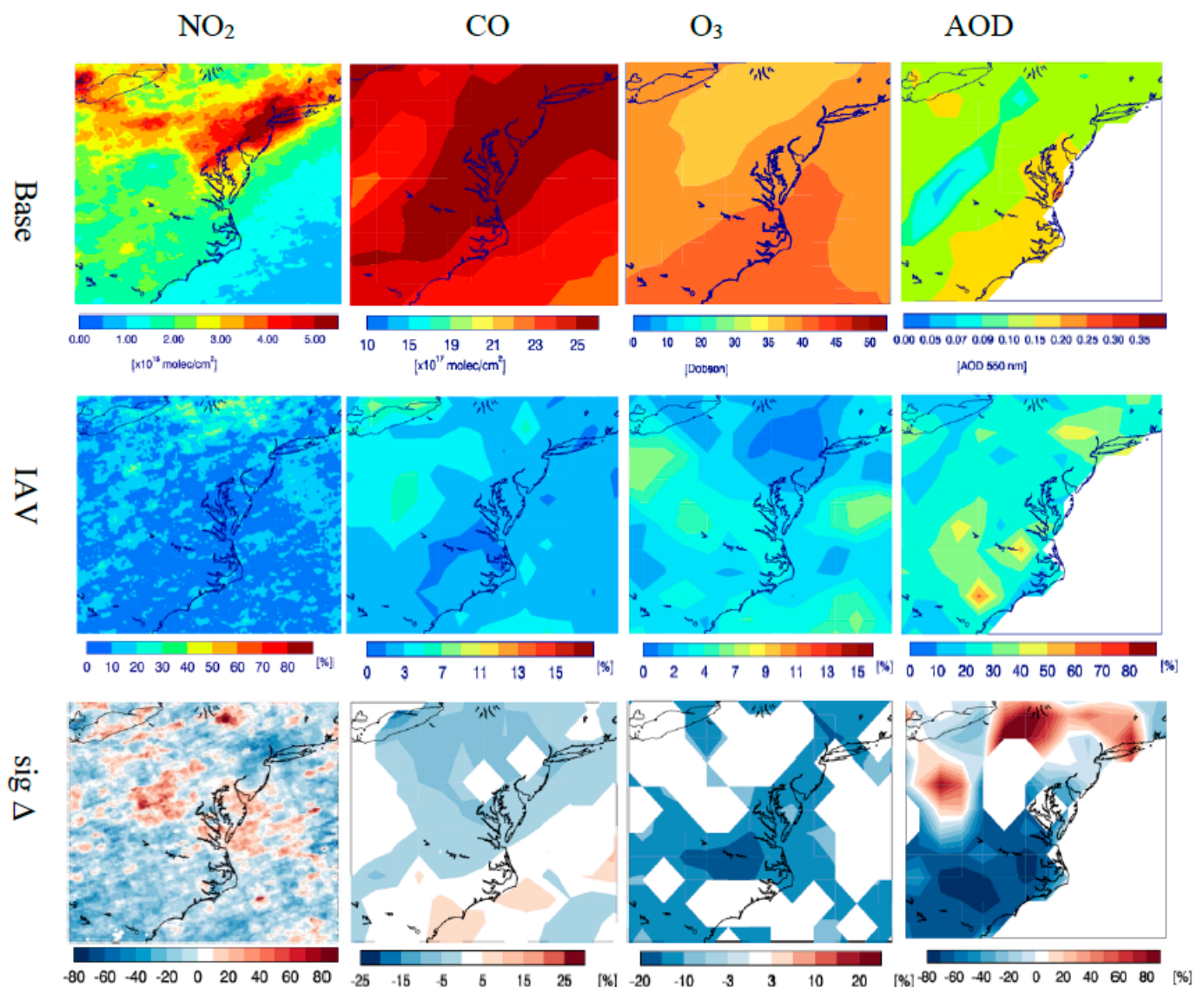
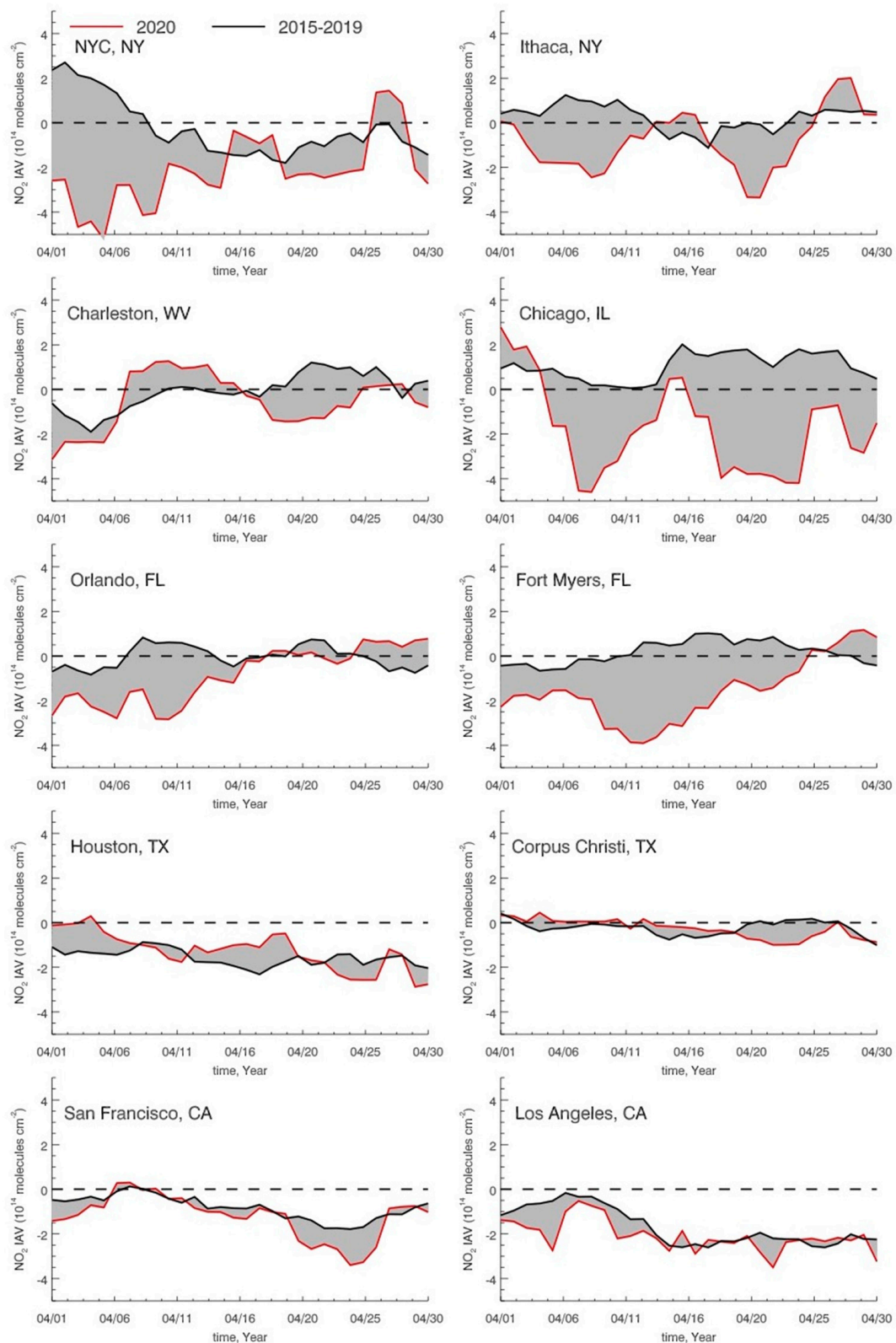


Figure 4. Same as Figure 3, but for the northeastern US.

$\text{O}_3$  levels increased from north to south over this region (toward higher temperature and solar radiation) with  $\text{O}_3$  tropospheric column (TCO) measuring 35 DU over NY and NJ and 40 DU to the south (on Virginia and North Carolina), see Figure 4.  $\text{O}_3$  IAV was very low, reaching  $\sim 2\%$  over NY, NJ, and DE. TCO was reduced by 15% in this region, which, given the small IAV in NYC, shows that the reduction of traffic volume in NYC was effective in improving AQ (ETR $\sim 13\%$ ). The decrease in  $\text{O}_3$  over NYC was also evident in the ozone IAV time series (Figure 6). No significant  $\text{O}_3$  changes could be seen over WV or PA (blank areas in Figure 4).



**Figure 5.** Interannual variability of  $\text{NO}_2$  tropospheric column during the base period (solid black line, 2015–2019) and during the lockdown period of the COVID-19 pandemic. The shaded areas represent the difference caused by lockdown measures.

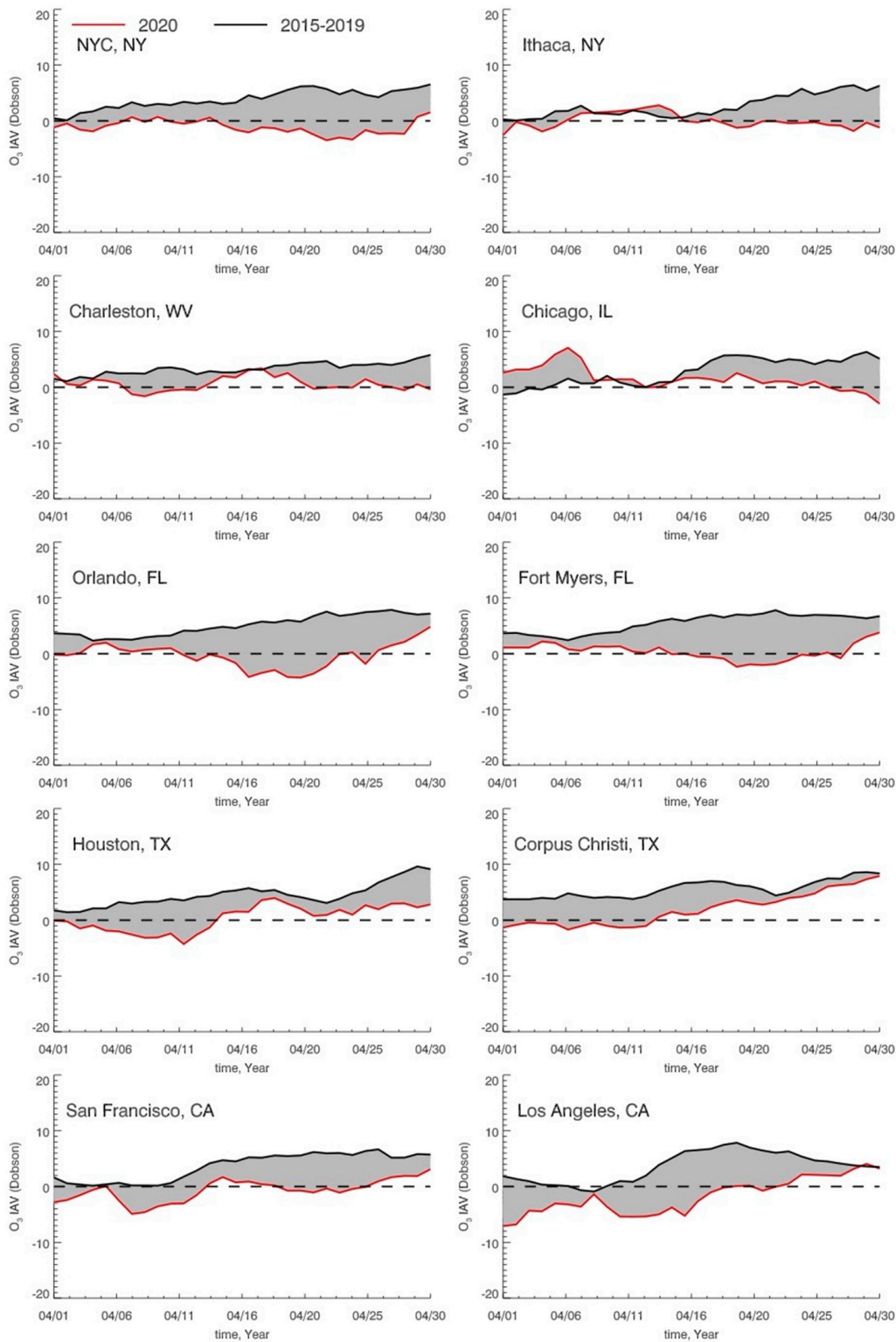


Figure 6. Same as Figure 5, but for O<sub>3</sub> tropospheric column.

The relative IAV of AOD over NYC, NJ, DE, and WV was about 40%, 25%, 20%, and 20%, respectively. AOD levels were not significantly changed over these states (considering the IAV and the negative bias of the MODIS DB product, see Section 3.2). However, AOD levels were significantly increased by up to 80% in WV and downwind of NYC, covering large parts of Connecticut and Pennsylvania. The decrease in CO levels but increased AOD in these regions indicate that these AOD increases were related to aged air masses

containing a large fraction of secondary organic (SOA) and, or inorganic aerosols from the hydrocarbon oxidation of gasses from nearby pollution sources, e.g., near Ohio River Valley to the west, downwind of NYC to the north [61–63]. The increased  $\text{NO}_2$  levels and decreased  $\text{O}_3$  levels are evidence of high  $\text{NO}_x$  conditions, under which the formation of  $\text{HNO}_3$  ( $\text{OH} + \text{NO}_2 \rightarrow \text{HNO}_3$ ) and alkyl nitrates ( $\text{RO}_2 + \text{NO} \rightarrow \text{RONO}_2$ ) would be enhanced.  $\text{RONO}_2$  and  $\text{HNO}_2$  can partition into particle-phase, which can constitute a large fraction of nitrate aerosol [53,64]. Similarly, over Charleston, WV, the increased AOD was likely due to the secondary aerosol formation from emitted OA from nearby chemical industries, especially given Charleston's confined geographic location in Kanawha Valley that allows for extended oxidation of OA under polluted condition [65]. The low relative change due to the pandemic in NJ of about  $-20\%$  was well within the IAV (see Figure 4). In contrast to  $\text{NO}_2$ , CO, and  $\text{O}_3$ , the reduction in traffic volume during the pandemic did not effectively reduce the aerosol load in NYC compared to the base period.

### 3.3.2. Midwest

Chicago, IL is a hot spot for traffic and industrial emissions and regularly experiences pollution events [66,67]. Traffic volume in the Chicago region, which includes the “collier” counties of Chicago: Cook, DuPage, Kane, Lake, McHenry, and Will, accounted for  $\sim 46\%$  of the traffic volume in the state of Illinois on March 11. The reduction in traffic volume, compared to 2019, was  $\sim 50\%$ , similar to that of the state of Illinois. In Chicago,  $\text{NO}_2$  IAV varied by  $\sim 15\%$ , and the  $\text{NO}_2$  relative change increased during the lockdown by  $\sim 20\%$ , i.e., only  $\sim 5\%$  beyond the IAV. The increase of  $\text{NO}_2$  during the pandemic indicates a pollution event that caused a slight increase in  $\text{NO}_2$  despite the reduction in traffic volume, which implies that the  $\text{NO}_2$  could have been higher without the lockdown and reduction in traffic volume during this time of the year. Although relatively small, the increase in  $\text{NO}_2$  also indicates high- $\text{NO}_x$  conditions. Furthermore, the small increase of  $\text{NO}_2$  over Chicago was very central, and the city center was surrounded by regions where  $\text{NO}_2$  was reduced (see Figure 7), and therefore cannot be reflected in the time series of the IAV in Figure 5, which covers a large  $1^\circ$  box around the city center. No effective reductions ( $\text{ETR} \leq 0$  in  $\text{NO}_2$ ) could be seen in Wisconsin or Indiana as well, given their higher IAV.

CO levels were also high in Chicago (see Figure 7) and IAVs were low, at  $\sim 3\%$ – $5\%$ . The relative change of CO in Chicago was highest in this region, reaching up to  $\sim 10\%$ , an evident CO increase during the pandemic, although marginal. No significant change can be seen in the northern city of Milwaukee. Similar to  $\text{NO}_2$ , the increase in CO (a primary emitted pollutant) despite the reduction in traffic is evidence of a pollution event that is often reported to be caused by the local meteorology in Chicago [67]. The increase of  $\text{NO}_2$  and CO despite the reduced traffic volume indicates that the reduction in traffic volume in these states is not effective in reversing the pollution course.

The tropospheric  $\text{O}_3$  column density was 35–37 DU. IAV was low at  $\sim 5\%$ .  $\text{sig } \Delta$  during the lockdown was at  $-15\%$  over the Chicago metropolitan area. The reduction in ozone over Chicago during the pandemic is a result of two concurrent effects: (1) the high- $\text{NO}_x$  conditions prevailed during the lockdown, which is mainly due to local meteorological conditions [67], possibly enforced by emissions from the nearby industrial park southeast of Chicago [68], and (2) The increase of  $\text{NO}_2$  under the prevailing high- $\text{NO}_x$  conditions causes a loss of OH [12,14], and thus less  $\text{O}_3$  photochemical formation.  $\text{O}_3$  reductions are also evident in the daily IAV plots, starting April 15 (Figure 5). Similar to  $\text{NO}_2$ , the small changes of  $\text{O}_3$  over central locations may not be optimally presented by the  $1^\circ$  box time series, especially if atmospheric changes are local such as changes in traffic emissions, and for species with a relatively high background such as  $\text{O}_3$  [14]. Therefore, the reduction in  $\text{O}_3$  was not related to the reduction in traffic volume but to the increase in  $\text{NO}_2$  levels from other local sources and, or meteorological conditions.

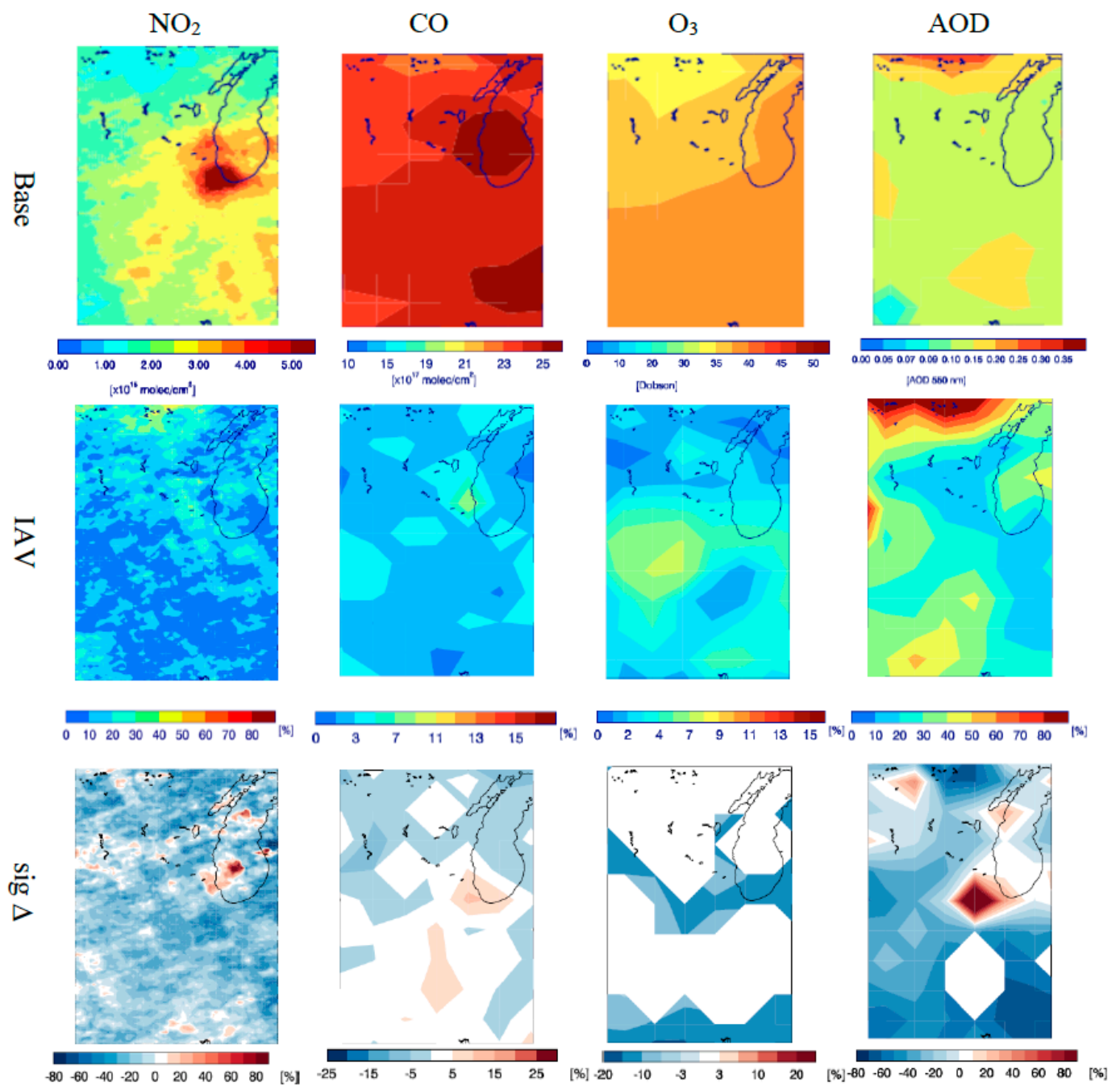


Figure 7. Same as Figure 3, but for the Midwest US.

While the AOD IAV is ~10%–30%, there is a significant increase of up to 80% in the AOD during the lockdown. The highest AOD is in the urban area of Chicago is impacted by the industrial area in the east and southeast [68]. Local meteorology plays an important role in the distribution and composition of pollutants in Chicago [67], and it seems that southwesterly winds with warm air and/or air stagnation causes high AOD in this region. The increase of NO<sub>2</sub>, CO, and AOD as a result of this pollution event led to increased inorganic aerosol (e.g., increased nitrate aerosol from increased OH + NO → HNO<sub>3</sub>) concentration in Chicago, consistent with previous analysis of aerosol formation in Chicago [67,68]. The small reduction of VOCs, CO, and NO<sub>x</sub> from the decrease in traffic volume was not sufficient to reverse the pollution event over Chicago, resulting in the persistent high aerosol event despite the reduction caused by the lockdown. Therefore, the impact of the pandemic related lockdown has been outweighed by meteorological conditions that led to higher NO<sub>x</sub>, CO, and aerosol load in Chicago. Therefore, we conclude that the reduction in traffic volume during the pandemic was not effective in reducing NO<sub>2</sub>, CO, and aerosol levels in Chicago because of the predominance of other pollution sources.

### 3.3.3. Southeast

In FL, which has a large traffic volume, the highest NO<sub>2</sub> levels were measured in the central part, near Orlando (Figure 8). The IAV of NO<sub>2</sub> levels (2015–2019) was also lowest (<10%) in the Tampa Bay region (in the central part) and reached up to ~10% in the north (near Jacksonville). *sig* Δ NO<sub>2</sub> during the lockdown period reached up to –30%, which shows that the reduction in traffic volume during the pandemic in FL was effective in reducing the NO<sub>2</sub> levels (ET = 20%), similar to NYC. The NO<sub>2</sub> reduction is also evident in the IAV time series (Figure 5) over Orlando and Fort Myers. The time series of the NO<sub>2</sub> over Jacksonville, Tampa, and Orlando (Figure S4) also showed a reduction during the lockdown period.

In FL, CO decreased from north to south while the IAV shows an almost opposite pattern (i.e., increasing from north to south). CO IAVs were ~3% in central and north FL but up to 7% in the south. The ETR was highest in central FL, reaching up to –15%, which is the most effective reduction observed in CO on the US eastern coast.

The O<sub>3</sub> levels in FL were almost homogeneous at ~40 DU. O<sub>3</sub> IAV is at 5%–7% overall. Significant O<sub>3</sub> reductions of 20% over central FL and 15% over north and south FL (Figure 8). Reductions in O<sub>3</sub> levels were also evident in the 1° box IAV time series (Figure 6). The concomitant decrease of NO<sub>2</sub>, CO, and O<sub>3</sub>, indicates NO sensitive conditions prevailing over FL, which distinguish FL from the other states on the US eastern coast. These results are also consistent with ground-based measurements in the state of FL [27].

AOD varied significantly, with IAV lowest in the north (10%–20%) and highest in central (30%–70%) and south FL (30%–40%). No significant differences in AOD can be detected in FL (Figure 8). In addition, [27] reported increased PM<sub>2.5</sub> levels in most of FL during the month of April of the lockdown period, which further supports previous literature reporting negative bias for the MODIS DB AOD product [42].

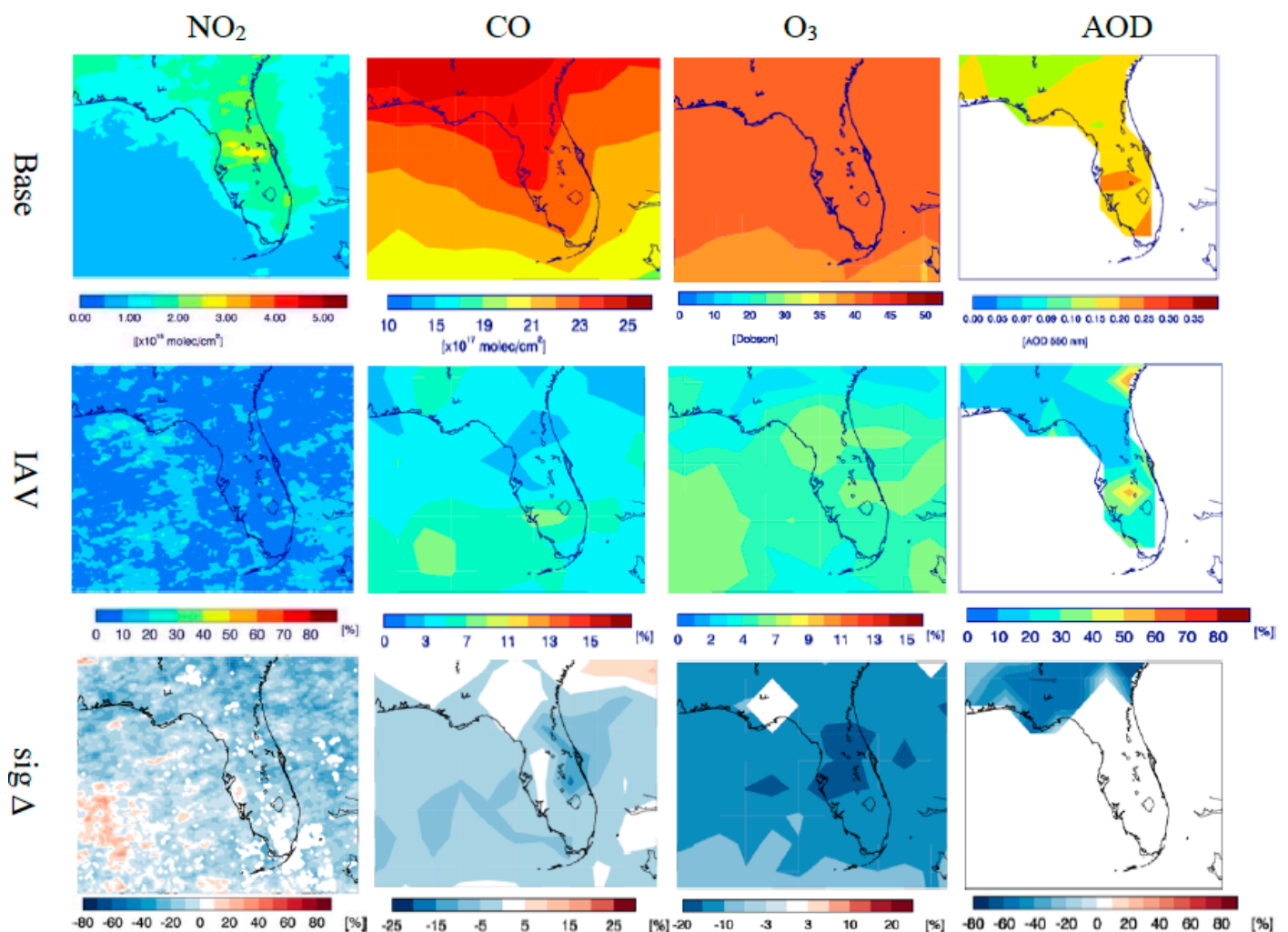


Figure 8. Same as Figure 3, but for the southeastern US (FL).

### 3.3.4. South

In TX,  $\text{NO}_2$  is highest near Houston, lower to the south near Corpus Christi. The IAV reached  $\sim 10\%$  near Houston but was lower ( $<10\%$ ) near Corpus Christi. Overall,  $\text{NO}_2$  significant reductions along the coast are within the IAV.  $\text{NO}_2$  changes in the 1<sup>o</sup> IAV time series are also very small compared to that of Orlando or NYC (Figure 5). Similarly, CO was reaching its maximum near Houston and slightly lower near Corpus Christi, with no ETR during the lockdown.

The tropospheric ozone column is decreased by 10% over southern TX, which is also within the IAV, i.e., no ETR (Figure 9). The AOD reduction was within the IAV over Houston but significantly increased over Corpus Christi, which may have been due to local events. Indeed, the Coastal Bend region of the TX coast has been reported to suffer frequent red tide blooms since the mid-1990s [69], which explains the vulnerable location of Corpus Christi that is almost at the vortex of the bend region. Red tide events cause high aerosol events that can be detected by remote sensing techniques [70,71]. The situation in TX is quite comparable to that of FL since photochemistry in both seems to have NO-sensitive conditions. Based on the above results, we conclude that a reduction in traffic volume in TX was not effective ( $\text{ETR} \leq 0$ ) in improving AQ due to the high IAV and the dominance of other pollution sources.

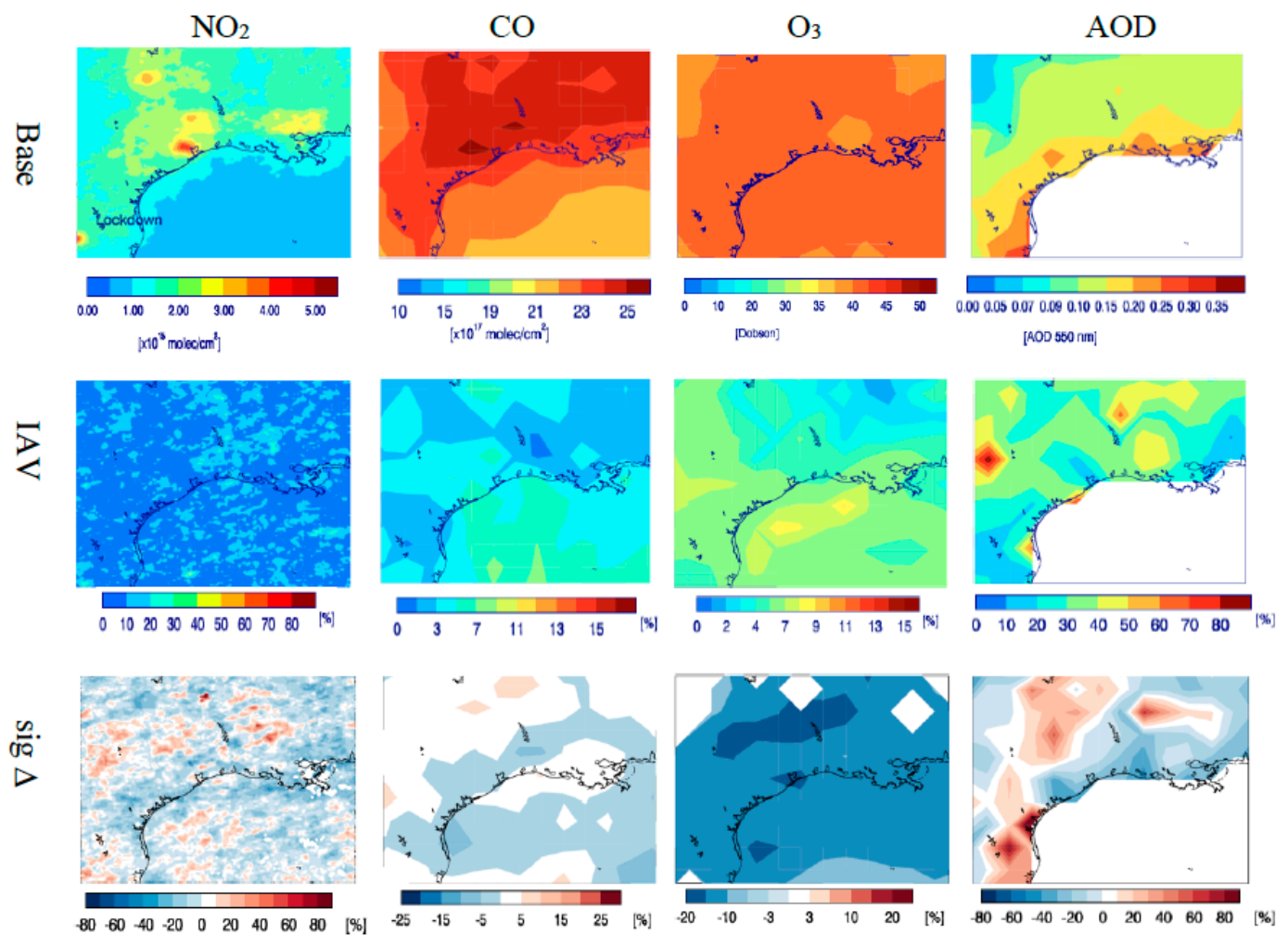


Figure 9. Same as Figure 3, but for the southern US.

### 3.3.5. West Coast

In California,  $\text{NO}_2$  IAV in Sacramento, San Francisco, and Los Angeles were 25%, 15%, and 10%, respectively. The relative changes during the lockdown were within the IAV with some isolated increases north of San Francisco and Sacramento (see Figure 10). Also, no reduction could be seen in the  $1^\circ$  IAV time series plots over San Francisco and Los Angeles (Figure 5). The US west coast frequently experiences long-range trans-pacific transport events from Asia and Europe that result in increased pollutants' levels in this region [55,72], which also peaks in late spring, coinciding with the pandemic lockdown incidence. The increase or no change in  $\text{NO}_2$  levels in San Francisco despite reduced  $\text{NO}_2$  emissions from their large traffic volume demonstrates that other sources dominate, e.g., meteorology and pollution events [14,73].  $\text{CO}$  levels are relatively high in San Francisco, and Los Angeles, IAVs were within 3% while relative changes in  $\text{CO}$  levels due to the pandemic are either insignificant or higher,  $\text{ETR}(\text{CO}) \leq 0$ .

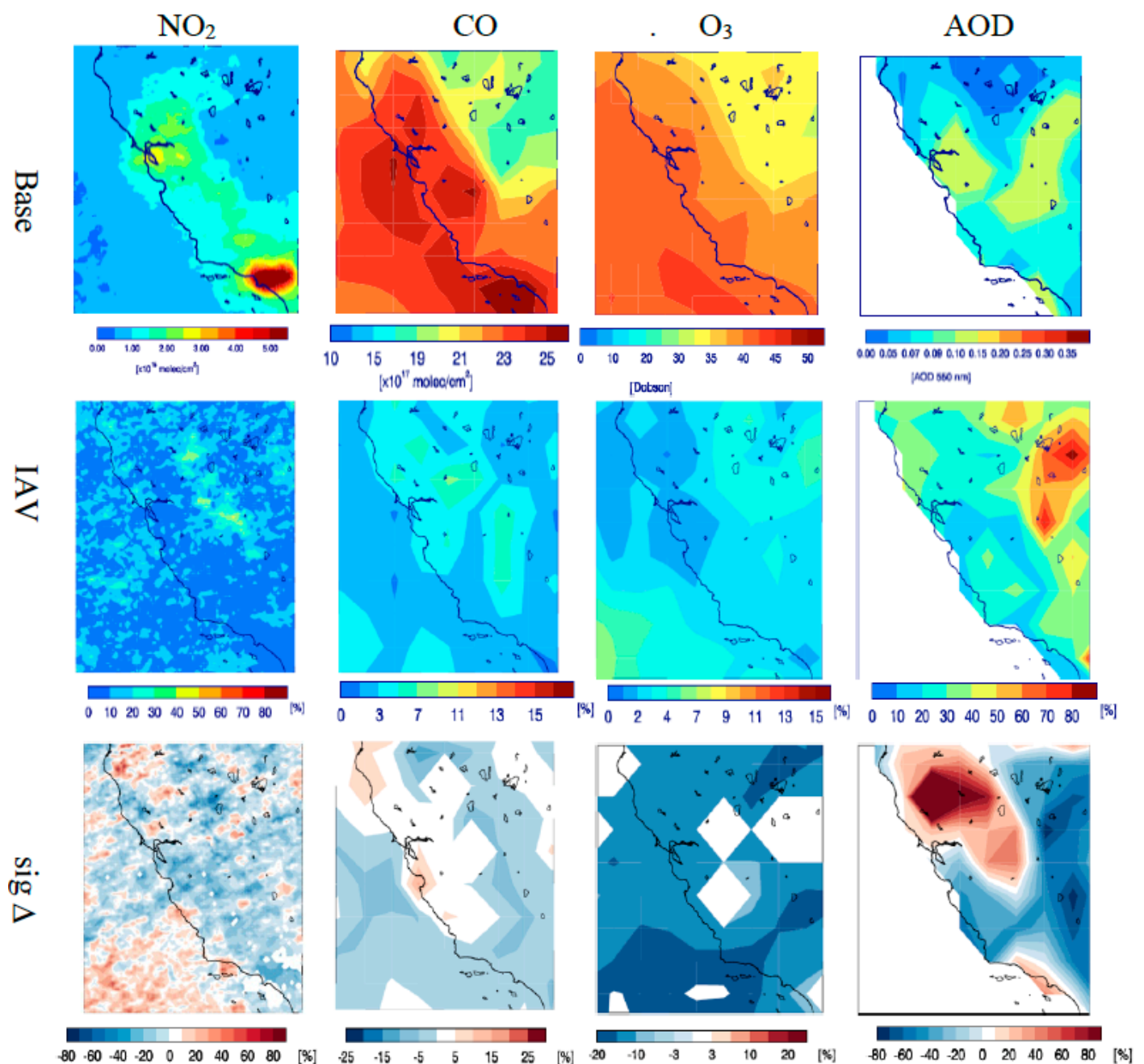


Figure 10. Same as Figure 3 but for the western coast.

Tropospheric ozone column levels can reach up to 43 DU on the western coast with relatively low IAV of up to 1%–2% on San Francisco and Los Angeles. Reductions in the ozone tropospheric column during the lockdown period is within 15% over San Francisco and Los Angeles (see Figures 5 and 10). As aforementioned, ozone is a photochemical product, and the increase of  $\text{NO}_2$  (north of San Francisco) under high- $\text{NO}_x$  conditions also decreases  $\text{O}_3$  formation.

AOD IAV during the base period (2010–2019) ranges between 10% and 30% over the western coast. However, there was a significant increase of AOD of up to 80% over San Francisco and to a much less extent of up to 30% over Los Angeles. Since these increases in AOD were not directly related to the reduced traffic volume during the pandemic, we report that  $\text{ETR}(\text{AOD}) \leq 0$  over CA.

#### 4. Conclusions

The COVID-19 pandemic has presented an unprecedented opportunity to investigate the impacts of a large-scale reduction in traffic volume on AQ. In this comprehensive study, we investigated the AQ status in the US during the pandemic using an ensemble of four remote sensing products for nitrogen dioxide tropospheric column, carbon monoxide atmospheric column, tropospheric ozone column, and AOD. We investigated and addressed the potential factors that might have masked the impacts of reduction in traffic volume and contributed to changes in AQ during the pandemic. We define the lockdown period pertinent to AQ as the period where the reduction in traffic volume reached an almost stable minimum level, based on actual data of traffic volume. We found that the reduction in traffic volume reached a quasi-stagnant level of 60%–40% during the lockdown period in most states. We determine a common effective lockdown period for all investigated states from 1 April to 1 May. During this time period, all traffic volumes were at their minimum.

In the NE US, the reduction of traffic volume was effective in reducing NO<sub>2</sub>, CO, and O<sub>3</sub> levels only in NYC, but not effective in other regions where other pollution sources dominate. In contrast to NO<sub>2</sub>, CO, and O<sub>3</sub>, reduction in traffic volume during the pandemic did not effectively reduce the AOD compared to the base period. In Chicago, the impact of the pandemic related lockdown has been outweighed by meteorological conditions and local emissions that lead to higher NO<sub>x</sub>, CO, and AOD. In FL, there has been a reduction of NO<sub>2</sub>, CO, and O<sub>3</sub>, especially in central FL, while AOD changes were not significant. Therefore, we conclude that the reduction in traffic volume during the pandemic in FL was effective in reducing the pollutant levels, except aerosols. In TX, NO<sub>2</sub>, CO, and O<sub>3</sub> levels were decreased as a result of the lockdown. However, the reductions were within the IAV. Therefore, we conclude that the reduction in traffic volume in Texas, despite significant, was not effective ( $ETR \leq 0$ ) in improving AQ due to the high IAV and the dominance of other pollution sources, especially in south TX. In CA, the reduction in traffic volume was not effective in improving AQ due to the dominance of other sources of pollution during the pandemic.

This large-scale experiment has allowed us to investigate the policy impacts of large-scale reduction in traffic emissions. Our results indicate that reduction of traffic volume during the pandemic was effective in improving air quality in regions where traffic is the main pollution source, such as in NYC and FL, while it was not effective in reducing pollution events where other pollution sources dominate, such as in IL, TX, and CA. Therefore, policies to reduce other emissions sources (e.g., industrial emissions) should also be considered, especially in places where the reduction in traffic volume was not effective in improving AQ.

**Supplementary Materials:** The following are available online at <https://www.mdpi.com/2072-4292/13/3/369/s1>, Figure S1: Statistical analyses of OMPS/MERRA2 TCO based on comparisons with ozonesonde TCO. The analyses were done using co-located daily measurements for years 2013–2017 and plotted versus sonde station latitude. Both OMPS/MERRA2 and ozonesonde TCO use the same tropopause pressure each day to derive the vertically integrated TCO columns. Upper left: Total number of daily matchups. Upper right: Offset differences (DU). Lower left: Standard deviations (DU) of their difference time series. Lower right: Temporal correlation between OMPS/MERRA2 and ozonesonde TCO time series, Figure S2: Selected daily time series comparisons between OMPS/MERRA2 TCO (blue curves) and ozonesonde TCO (red boxes) for several NH and SH sonde station sites for years when there were 2–3 years of mostly continuous weekly ozonesonde measurements. Included in each panel are the OMPS minus sonde offset (in DU) and the standard deviation (in DU) of their difference time series for 2015–2017, Figure S3: Selected monthly TCO (in DU) time series comparisons at several city sites (three in NH, three in SH) between OMI/MLS (black curves) and OMPS/MERRA2 (red curves). One site shown is Washington DC (upper middle panel) that was located over the eastern coast of the United States. The OMI/MLS TCO measurements (Ziemke et al., 2006) use a different tropopause pressure definition (WMO 2K/km lapse rate definition) than OMPS/MERRA2 TCO. However, these different tropopause pressure definitions cannot produce more than ~1–2 DU time series differences between monthly OMI/MLS

and OMPS/MERRA2 TCO, Figure S4: OMPS/MERRA2 TCO minus OMI/MLS TCO average offsets and calculated  $\pm 1$  standard deviations of their differences (shown as vertical bars). Data points for this statistical analysis are accrued over both space (longitude) and time (month) in 5-degree latitude bands. Mean offsets are small, at most 2–3 DU everywhere except in mid-high latitudes in the SH where the average offset was about –5 DU. The cause for this offset in the SH was not unexpected due to having two different TCO products with very different algorithms and also instrument calibration differences that can have a latitude dependence. The difference standard deviations as shown by the vertical bars are also small at only about 2–3 DU at all latitudes. These small standard deviations show that the two TCO products are capturing very similar space-time variability, Figure S5: OMPS/MERRA2 TCO (in DU) seasonal climatology global maps derived using data from January 2012–December 2019. Seasonal means (indicated) are for December-January-February (DJF), March-April-May (MAM), June-July-August (JJA), and September-October-November (SON). Figure S6: Top panel: Mean pollutant levels during the base period (Base, 2015–2019); Middle panel: mean annual variability (due to trends and interannual variability) of the base period; Bottom panel: Relative change during the lockdown period of the COVID-19 pandemic, Figure S7: 15-days running average of NO<sub>2</sub> tropospheric column during the base period (solid black line, 2015–2019); mean standard deviation of the base period (error bars); and NO<sub>2</sub> tropospheric column during the lockdown period of the COVID-19 pandemic. The time series is an average of a 1° box (lon × lat) from the respective city center and therefore may have been biased with nearby pollution sources, Figure S8: Same as S7 but for O<sub>3</sub> tropospheric column, Figure S9: Mean NO<sub>2</sub> during the base (solid black line) period (2015–2019) compared to 2020 (solid red line).

**Author Contributions:** Y.F.E.: Conceptualization, Investigation, Methodology, Validation, Writing. H.C.K.: Investigation, Methodology. J.R.Z.: O<sub>3</sub> OMPS data, Investigation, Validation, Writing. S.A.P.: data and figures for the traffic and COVID-19 cases, writing. All authors have read and agreed to the published version of the manuscript.

**Funding:** This research was funded by the USF COVID-19 Rapid Response Grant Program, grant number 100431, and the NSF AGS, grant number 1900795.

**Institutional Review Board Statement:** Not applicable.

**Informed Consent Statement:** Not applicable.

**Data Availability Statement:** The data presented in this study are openly available as outlined in Section 2.2.

**Conflicts of Interest:** The authors declare no conflict of interest.

## References

1. WHO. The World Health Organization. Coronavirus Disease (COVID-19) Pandemic. Available online: <https://www.who.int/emergencies/diseases/novel-coronavirus-2019> (accessed on 10 October 2020).
2. CDC. Center for Disease Control and Prevention. Available online: <https://COVID.cdc.gov/COVID-data-tracker/> (accessed on 12 October 2020).
3. Hopkins, J. Coronavirus Resource Center. Available online: <https://coronavirus.jhu.edu> (accessed on 1 December 2020).
4. De Haas, M.; Faber, R.; Hamersma, M. How COVID-19 and the Dutch “intelligent lockdown” change activities, work and travel behaviour: Evidence from longitudinal data in the Netherlands. *Transp. Res. Interdiscip. Perspect.* **2020**, *6*, 100150. [CrossRef]
5. Beck, M.J.; Hensher, D.A. Insights into the impact of COVID-19 on household travel and activities in Australia—The early days under restrictions. *Transp. Policy* **2020**, *96*, 76–93. [CrossRef] [PubMed]
6. Parr, S.; Wolshon, B.; Renne, J.; Murray-Tuite, P.; Kim, K. Traffic Impacts of the COVID-19 Pandemic: Statewide Analysis of Social Separation and Activity Restriction. *Nat. Hazards Rev.* **2020**, *21*. [CrossRef]
7. Carteni, A.; Di Francesco, L.; Martino, M. How mobility habits influenced the spread of the COVID-19 pandemic: Results from the Italian case study. *Sci. Total Environ.* **2020**, *741*, 140489. [CrossRef] [PubMed]
8. Hadjidemetriou, G.M.; Sasidharan, M.; Kouyialis, G.; Parlikad, A.K. The impact of government measures and human mobility trend on COVID-19 related deaths in the UK. *Transp. Res. Interdisc. Perspect.* **2020**, *6*, 100167.
9. Colville, R.N.; Hutchinson, E.J.; Mindell, J.S.; Warren, R.F. The transport sector as a source of air pollution. *Atmos. Environ.* **2001**, *35*, 1537–1565. [CrossRef]
10. O’Driscoll, R.; Stettler, M.E.J.; Molden, N.; Oxley, T.; ApSimon, H.M. Real world CO<sub>2</sub> and NO<sub>x</sub> emissions from 149 euro 5 and 6 diesel, gasoline and hybrid passenger cars. *Sci. Total Environ.* **2018**, *621*, 282–290. [CrossRef]

11. Vojtišek-Lom, M.; Beranek, V.; Klír, V.; Jindra, P.; Pechout, M.; Voříšek, T. On-road and laboratory emissions of NO, NO<sub>2</sub>, NH<sub>3</sub>, N<sub>2</sub>O and CH<sub>4</sub> from late-model EU light utility vehicles: Comparison of diesel and CNG. *Sci. Total Environ.* **2018**, *616*, 774–784. [[CrossRef](#)]
12. Elshorbany, Y.F.; Kleffmann, J.; Kurtenbach, R.; Rubio, R.; Lissi, E.; Villena, G.; Rickard, A.R.; Pilling, M.J.; Wiesen, P. Summertime Photochemical Ozone Formation in Santiago de Chile. *Atmos. Environ.* **2009**, *43*, 6398–6420. [[CrossRef](#)]
13. Liu, F.; Page, A.; Strode, S.A.; Yoshida, Y.; Choi, S.; Zheng, B.; Lamsal, L.N.; Li, C.; Krotkov, N.A.; Eskes, H.; et al. Abrupt decline in tropospheric nitrogen dioxide over China after the outbreak of COVID-19. *Sci. Adv.* **2020**, *6*, 28. [[CrossRef](#)]
14. Venter, Z.S.; Aunan, K.; Chowdhury, S.; Lelieveld, J. COVID-19 lockdowns cause global air pollution declines. *Natl. Acad. Sci.* **2020**, *117*, 18984–18990. [[CrossRef](#)] [[PubMed](#)]
15. Putaud, J.-P.; Pozzoli, L.; Pisoni, E.; Martins Dos Santos, S.; Lagler, F.; Lanzani, G.; Dal Santo, U.; Colette, A. Impacts of the COVID-19 lockdown on air pollution at regional and urban background sites in northern Italy. *Atmos. Chem. Phys. Discuss.* **2020**, in review. [[CrossRef](#)]
16. Pathakoti, M.; Muppalla, A.; Hazra, S.; Dangeti, M.; Shekhar, R.; Jella, S.; Mullapudi, S.S.; Andugulapati, P.; Vijayasundaram, U. An assessment of the impact of a nation-wide lockdown on air pollution—A remote sensing perspective over India. *Atmos. Chem. Phys. Discuss.* **2020**, in review. [[CrossRef](#)]
17. Chen, L.-W.A.; Chien, L.-C.; Li, Y.; Lin, G. Nonuniform impacts of COVID-19 lockdown on air quality over the United States. *Sci. Total Environ.* **2020**, *745*, 141105. [[CrossRef](#)]
18. Zangari, S.; Hill, D.T.; Charette, A.T.; Mirowsky, J.E. Air quality changes in New York City during the COVID-19 pandemic. *Sci. Total Environ.* **2020**, *742*, 140496. [[CrossRef](#)]
19. Huang, G.; Sun, K. Non-Negligible impacts of clean air regulations on the reduction of tropospheric NO<sub>2</sub> over East China during the COVID-19 pandemic observed by OMI and TROPOMI. *Sci. Total Environ.* **2020**, *745*. [[CrossRef](#)]
20. Bauwens, M.; Compernelle, S.; Stavrou, T.; Müller, J.; Gent, J.; Eskes, H.; Levelt, P.F.; van der A, R.; Veefkind, J.P.; Vlietinck, J.; et al. Impact of Coronavirus Outbreak on NO<sub>2</sub> Pollution Assessed Using TROPOMI and OMI Observations. *Geophys. Res. Lett.* **2020**, *47*. [[CrossRef](#)]
21. Tobías, A.; Carnerero, C.; Reche, C.; Massagué, J.; Via, M.; Minguillón, M.C.; Alastuey, A.; Querol, X. Changes in air quality during the lockdown in Barcelona (Spain) one month into the SARS-CoV-2 epidemic. *Sci. Total Environ.* **2020**, *726*, 138540. [[CrossRef](#)]
22. Zheng, H.; Kong, S.; Chen, N.; Yan, Y.; Liu, D.; Zhu, B.; Xu, K.; Cao, W.; Ding, Q.; Lan, B.; et al. Significant changes in the chemical compositions and sources of PM<sub>2.5</sub> in Wuhan since the city lockdown as COVID-19. *Sci. Total Environ.* **2020**, *739*, 140000. [[CrossRef](#)]
23. Ding, J.; van der A, R.J.; Eskes, H.; Mijling, B.; Stavrou, T.; van Geffen, J.; Veefkind, P. NO<sub>x</sub> emissions reduction and rebound in China due to the COVID-19 crisis. *Earth Space Sci. Open Arch.* **2020**, *47*. [[CrossRef](#)]
24. Cazorla, M.; Herrera, E.; Palomeque, E.; Saud, N. What the COVID-19 lockdown revealed about photochemistry and ozone production in Quito, Ecuador. *Atmos. Pollut. Res.* **2020**, in press. [[CrossRef](#)] [[PubMed](#)]
25. Huang, X.; Ding, A.; Gao, J.; Zheng, B.; Zhou, D.; Qi, X.; Tang, R.; Wang, J.; Ren, C.; Nie, W.; et al. Enhanced secondary pollution offset reduction of primary emissions during COVID-19 lockdown in China. *Natl. Sci. Rev.* **2020**, *1–9*, nwa137. [[CrossRef](#)]
26. Wang, P.; Chen, K.; Zhu, S.; Wang, P.; Zhang, H. Severe air pollution events not avoided by reduced anthropogenic activities during COVID-19 outbreak. *Resour. Conserv. Recycl.* **2020**, *158*, 104814. [[CrossRef](#)] [[PubMed](#)]
27. El-Sayed, M.; Elshorbany, Y.; Koehler, K. On the impact of COVID-19 pandemic on air quality in FL. 2021; in preparation.
28. Bekbulat, B.; Apte, J.S.; Millet, D.B.; Robinson, A.; Wells, K.C.; Marshall, J.D. PM<sub>2.5</sub> and Ozone Air Pollution Levels Have Not Dropped Consistently Across the US Following Societal COVID Response. *ChemRxiv* **2020**. [[CrossRef](#)]
29. Federal Highway Administration (FHWA). Highway Performance Monitoring System (HPMS). Available online: <https://www.fhwa.dot.gov/policyinformation/hpms/hpmsprimer.cfm> (accessed on 13 July 2020).
30. Shilling, F. *Special Report (Update): Impact of COVID19 Mitigation on Numbers and Costs of California Traffic Crashes*; Road Ecology Center: Davis, CA, USA, 2020; Available online: [https://roadecology.ucdavis.edu/files/content/projects/COVID\\_CHIPs\\_Impacts\\_updated\\_415\\_1.pdf](https://roadecology.ucdavis.edu/files/content/projects/COVID_CHIPs_Impacts_updated_415_1.pdf) (accessed on 1 October 2020).
31. Lamsal, L.N.; Krotkov, N.A.; Vasilkov, A.; Marchenko, S.; Qin, W.; Yang, E.-S.; Fasnacht, Z.; Joiner, J.; Choi, S.; Haffner, D.; et al. OMI/Aura Nitrogen Dioxide Standard Product with Improved Surface and Cloud Treatments. *Atmos. Meas. Tech. Discuss.* **2020**, in review. [[CrossRef](#)]
32. Barret, B.; DeMazière, M.; Mahieu, E. Ground-Based FTIP measurements of CO from Jungfraujoch: Characterisation and comparison with in situ surface and MOPITT data. *Atmos. Chem. Phys.* **2003**, *3*, 2217. [[CrossRef](#)]
33. Buchholz, R.R.; Deeter, M.N.; Worden, H.M.; Gille, J.; Edwards, D.P.; Hannigan, J.W.; Jones, N.B.; Paton-Walsh, C.; Griffith, D.W.T.; Smale, D.; et al. Validation of MOPITT carbon monoxide using ground-based Fourier transform infrared spectrometer data from NDACC. *Atmos. Meas. Tech.* **2017**, *10*, 1927–1956. [[CrossRef](#)]
34. Wei, J.; Li, Z.; Peng, Y.; Sun, L. MODIS Collection 6.1 aerosol optical depth products over land and ocean: Validation and comparison. *Atmos. Environ.* **2019**, *201*, 428–440. [[CrossRef](#)]
35. Hsu, N.C.; Jeong, M.-J.; Bettenhausen, C.; Sayer, A.M.; Hansell, R.; Seftor, C.S.; Huang, J.; Tsay, S.-C. Enhanced Deep Blue Aerosol Retrieval Algorithm: The Second Generation. *J. Geophys. Res.* **2013**, *118*. [[CrossRef](#)]
36. Sayer, A.M.; Hsu, N.C.; Lee, J.; Kim, W.V.; Dutcher, S.T. Validation, stability, and consistency of MODIS collection 6.1 and VIIRS version 1 Deep Blue aerosol data over land. *J. Geophys. Res. Atmos.* **2019**, *124*, 4658–4688. [[CrossRef](#)]

37. Ziemke, J.R.; Chandra, S.; Duncan, B.N.; Froidevaux, L.; Bhartia, P.K.; Levelt, P.F.; Waters, J.W. Tropospheric ozone determined from Aura OMI and MLS: Evaluation of measurements and comparison with the Global Modeling Initiative's Chemical Transport Model. *J. Geophys. Res.* **2006**, *111*, D19303. [[CrossRef](#)]
38. McPeters, R.D.; Frith, S.M.; Kramarova, N.A.; Ziemke, J.R.; Labow, G.L. OMI total column ozone: Extending the long-term data record. *Atmos. Meas. Tech.* **2019**, *8*, 4845–4850. [[CrossRef](#)]
39. Gelaro, R.; McCarty, W.; Suárez, M.J.; Todling, R.; Molod, A.; Takacs, L.; Randles, C.A.; Darmenov, A.; Bosilovich, M.G.; Reichle, R.; et al. The Modern-Era Retrospective Analysis for Research and Applications, Version 2 (MERRA-2). *J. Clim.* **2017**, *30*, 5419–5454. [[CrossRef](#)]
40. Tropospheric Ozone Public Domain. Available online: <https://gmao.gsfc.nasa.gov/reanalysis/MERRA-2> (accessed on 3 December 2020).
41. Lee, H.; Garay, M.J.; Kalashnikova, O.V.; Yu, Y.; Gibson, P.B. How Long should the MISR Record Be when Evaluating Aerosol Optical Depth Climatology in Climate Models? *Remote Sens.* **2018**, *10*, 1326. [[CrossRef](#)]
42. Shi, H.; Xiao, Z.; Ma, H.; Tian, X. Evaluation of MODIS and two reanalysis aerosol optical depth products over AERONET sites. *Atmos. Res.* **2019**, *220*, 75–80. [[CrossRef](#)]
43. Devore, J. *Probability and Statistics for Engineering and the Sciences*, 8th ed.; California Polytechnic State University: San Luis Obispo, CA, USA, 2012; ISBN 13-978-0-538-73352-6.
44. Huang, N.E.; Shen, Z.; Long, S.R.; Wu, M.C.; Shih, H.H.; Zheng, Q.; Yen, N.-C.; Chao, C. The Empirical Mode Decomposition and the Hilbert Spectrum for Nonlinear and Non-Stationary Time Series Analysis. *Proc. R. Soc. Lond.* **1998**, *454*, 903–995. [[CrossRef](#)]
45. Wu, Z.; Norden, E.H.; Long, S.R.; Peng, C.K. On the trend, detrending, and variability of nonlinear and nonstationary time series. *Proc. Natl. Acad. Sci. USA* **2007**, *104*, 14889–14894. [[CrossRef](#)]
46. Jiang, C.; Ryu, Y.; Fang, H.; Myneni, R.; Claverie, M.; Zhu, Z. Inconsistencies of interannual variability and trends in long-term satellite leaf area index products. *Glob. Chang. Biol.* **2017**, *23*, 4133–4146. [[CrossRef](#)]
47. Jones, C.; Kammen, D.M. Spatial Distribution of U.S. Household Carbon Footprints Reveals Suburbanization Undermines Greenhouse Gas Benefits of Urban Population Density. *Environ. Sci. Technol.* **2014**, *48*, 895–902. [[CrossRef](#)]
48. US Department of Transportation. Transportation GHG Emissions and Trends. Available online: <https://www.transportation.gov/sustainability/climate/transportation-ghg-emissions-and-trends> (accessed on 22 October 2020).
49. Gately, C.; Hutyra, L.R.; Wing, I.S. *DARTE Annual On-Road CO<sub>2</sub> Emissions on a 1-km Grid, Conterminous USA, V2, 1980–2017*; ORNL DAAC: Oak Ridge, TN, USA, 2019. [[CrossRef](#)]
50. Elshorbany, Y.F.; Duncan, B.N.; Strode, S.A.; Wang, J.S.; Kouatchou, J. The description and validation of the computationally Efficient CH<sub>4</sub>–CO–OH (ECCOHv1.01) chemistry module for 3-D model applications. *Geosci. Model Dev.* **2016**, *9*, 799–822. [[CrossRef](#)]
51. Hoesly, R.M.; Smith, S.J.; Feng, L.; Klimont, Z.; Janssens-Maenhout, G.; Pitkanen, T.; Seibert, J.J.; Vu, L.; Andres, R.J.; Bolt, R.M.; et al. Historical (1750–2014) anthropogenic emissions of reactive gases and aerosols from the Community Emission Data System (CEDS). *Geosci. Model Dev.* **2018**, *11*, 369–408. [[CrossRef](#)]
52. Krotkov, N.A.; McLinden, C.A.; Li, C.; Lamsal, L.N.; Celarier, E.A.; Marchenko, S.V.; Swartz, W.H.; Bucsela, E.J.; Joiner, J.; Duncan, B.N.; et al. Aura OMI observations of regional SO<sub>2</sub> and NO<sub>2</sub> pollution changes from 2005 to 2015. *Atmos. Chem. Phys.* **2016**, *16*, 4605–4629. [[CrossRef](#)]
53. Elshorbany, Y.F.; Crutzen, P.J.; Steil, B.; Pozzer, A.; Tost, H.; Lelieveld, J. Global and regional impacts of HONO on the chemical composition of clouds and aerosols. *Atmos. Chem. Phys.* **2014**, *14*, 1167–1184. [[CrossRef](#)]
54. Simon, H.; Reff, A.; Wells, B.; Xing, J.; Frank, N. Ozone Trends Across the United States over a Period of Decreasing NO<sub>x</sub> and VOC Emissions. *Environ. Sci. Technol.* **2015**, *49*, 186–195. [[CrossRef](#)]
55. Jaffe, D.A.; Cooper, O.R.; Fiore, A.M.; Henderson, B.H.; Tonnesen, G.S.; Russell, A.G.; Henze, D.K.; Langford, A.O.; Lin, M.; Moore, T. Scientific assessment of background ozone over the U.S.: Implications for air quality management. *Elem. Sci. Anth.* **2018**, *6*, 56. [[CrossRef](#)]
56. Yang, Q.; Yuan, Q.; Yue, L.; Li, T.; Shen, H.; Zhang, L. The relationships between PM<sub>2.5</sub> and aerosol optical depth (AOD) in mainland China: About and behind the spatio-temporal variations. *Environ. Pollut.* **2019**, *248*, 526–535. [[CrossRef](#)]
57. Stirnberg, R.; Cermak, J.; Andersen, H. An Analysis of Factors Influencing the Relationship between Satellite-Derived AOD and Ground-Level PM<sub>10</sub>. *Remote Sens.* **2018**, *10*, 1353. [[CrossRef](#)]
58. Berman, J.D.; Ebisu, K. Changes in U.S. air pollution during the COVID-19 pandemic. *Sci. Total Environ.* **2020**, *739*, 139864. [[CrossRef](#)]
59. Roy, P. Atmospheric Smog Modeling, Using EOS Satellite ASTER Image Sensor, with Feature Extraction for Pattern Recognition Techniques and Its Correlation with In-Situ Ground Sensor Data. Ph.D. Thesis, Marshall University, Huntington, WV, USA, 2007. Available online: <https://mds.marshall.edu/cgi/viewcontent.cgi?referer=https://www.google.com/&httpsredir=1&article=1817&context=etd> (accessed on 27 October 2020).
60. Lewis, C.W.; Macias, E.S. Composition of size-fractionated aerosol in Charleston, West Virginia. *Atmos. Environ.* **1979**, *14*, 185–194. [[CrossRef](#)]
61. Kleinman, L.I.; Daum, P.H.; Lee, Y.-N.; Nunnermacker, L.J.; Springston, S.R.; Weinstein-Lloyd, J.; Rudolph, J. A comparative study of ozone production in 5 U.S. metropolitan areas. *J. Geophys. Res.* **2005**, *110*, D02301. [[CrossRef](#)]

62. Shah, V.; Jaeglé, L.; Jimenez, J.L.; Schroder, J.C.; Campuzano-Jost, P.; Campos, T.L.; Reeves, J.M.; Stell, M.; Brown, S.S.; Lee, B.H.; et al. Widespread pollution from secondary sources of organic aerosols during winter in the Northeastern United States. *Geophys. Res. Lett.* **2019**, *46*, 2974–2983. [[CrossRef](#)]
63. Schroder, J.C.; Campuzano-Jost, P.; Day, D.A.; Shah, V.; Larson, K.; Sommers, J.M.; Sullivan, A.P.; Campos, T.; Reeves, J.M.; Hills, A.; et al. Sources and secondary production of organic aerosols in the northeastern United States during WINTER. *J. Geophys. Res. Atmos.* **2018**, *123*, 7771–7796. [[CrossRef](#)]
64. Li, K.; Liggio, J.; Han, C.; Liu, Q.; Moussa, S.G.; Lee, P.; Li, S.-M. Understanding the Impact of High-NO<sub>x</sub> Conditions on the Formation on Secondary Organic Aerosol in the Photooxidation of Oil Sand-Related Precursors. *Environ. Sci. Technol.* **2019**, *53*, 14420–14429. [[CrossRef](#)] [[PubMed](#)]
65. Cohen, M.A.; Ryan, P.B.; Spengler, J.D.; Özkaynak, H.; Hayes, C. Source-Receptor study of volatile organic compounds and particulate matter in the Kanawha Valley, WV—I. Methods and descriptive statistics. *Atmos. Environ.* **1991**, *25B*, 79–93. [[CrossRef](#)]
66. Lyons, W.A. The climatology and prediction of the Chicago Lake Breeze. *J. Appl. Meteorol.* **1972**, *11*, 1259–1270. [[CrossRef](#)]
67. Fosco, T.; Schmeling, M. Aerosol ion concentration dependence on atmospheric conditions in Chicago. *Atmos. Environ.* **2006**, *40*, 6638–6649. [[CrossRef](#)]
68. Xiang, S.; Hu, Z.; Zhai, W.; Wen, D.; Noll, K.E. Concentration of Ultrafine Particles near Roadways in an Urban Area in Chicago, Illinois. *Aerosol. Air Qual. Res.* **2018**, *18*, 895–903. [[CrossRef](#)]
69. Tominack, S.A.; Coffey, K.Z.; Yoskowitz, D.; Sutton, G.; Wetz, M.S. An assessment of trends in the frequency and duration of *Karenia brevis* red tide blooms on the South Texas coast (western Gulf of Mexico). *PLoS ONE* **2020**, *15*, e0239309. [[CrossRef](#)]
70. Cheng, Y.S.; Villareal, T.A.; Zhou, Y.; Gao, J.; Pierce, R.H.; Wetzel, D.; Naar, J.; Baden, D.G. Characterization of red tide aerosol on the Texas coast. *Harmful Algae* **2005**, *4*, 87–94. [[CrossRef](#)]
71. Hu, C.; Muller-Karger, F.E.; Taylor, C.J.; Carder, K.L.; Kelble, C.; Johns, E.; Heil, C.A. Red tide detection and tracing using MODIS fluorescence data: A regional example in SW FL coastal waters. *Remote Sens. Environ.* **2005**, *97*, 311–321. [[CrossRef](#)]
72. Faloon, I.C.; Chiao, S.; Eiserloh, A.J.; Alvarez, R.J.; Kirgis, G.; Langford, A.O.; Senff, C.J.; Caputi, D.; Hu, A.; Iraci, L.T.; et al. The California Baseline Ozone Transport Study (CABOTS). *Bull. Am. Meteor. Soc.* **2020**, *101*, E427–E445. [[CrossRef](#)]
73. Zhao, K.; Bao, Y.; Huang, J.; Wu, Y.; Moshary, F.; Arend, M.; Wang, Y.; Lee, X. A high-resolution modeling study of a heat wave-driven ozone exceedance event in New York City and surrounding regions. *Atmos. Environ.* **2019**, *199*. [[CrossRef](#)]